Article

Free Energy Landscape of Rim-Pore Expansion in Membrane Fusion

Herre Jelger Risselada,[1,2,*] Yuliya Smirnova,[3] and Helmut Grubmüller[1]
[1]Theoretical Molecular Biophysics Group, Max-Planck-Institute for Biophysical Chemistry, Göttingen, Germany; [2]Leibniz Institute of Surface Modification, Leipzig, Germany; and [3]Georg August University, Institute for Theoretical Physics, Göttingen, Germany

ABSTRACT The productive fusion pore in membrane fusion is generally thought to be toroidally shaped. Theoretical studies and recent experiments suggest that its formation, in some scenarios, may be preceded by an initial pore formed near the rim of the extended hemifusion diaphragm (HD), a rim-pore. This rim-pore is characterized by a nontoroidal shape that changes with size. To determine this shape as well as the free energy along the pathway of rim-pore expansion, we derived a simple analytical free energy model. We argue that dilation of HD material via expansion of a rim-pore is favored over a regular, circular pore. Further, the expanding rim-pore faces a free energy barrier that linearly increases with HD size. In contrast, the tension required to expand the rim-pore decreases with HD size. Pore flickering, followed by sudden opening, occurs when the tension in the HD competes with the line energy of the rim-pore, and the rim-pore reaches its equilibrium size before reaching the critical pore size. The experimental observation of flickering and closing fusion pores (kiss-and-run) is very well explained by the observed behavior of rim-pores. Finally, the free energy landscape of rim-pore expansion/HD dilation may very well explain why some cellular fusion reactions, in their attempt to minimize energetic costs, progress via alternative formation and dilation of microscopic hemifusion intermediates.

INTRODUCTION

Over the past 20 years it has become widely accepted that membrane fusion proceeds through a hemifusion state which eventually develops into a fusion pore. The structure of the fusion pore, which is experimentally characterized by the measurement of electric conductance or the observed flux of fluorescence dye, is generally thought to be toroidal. Fusion pores have been observed to either close (kiss-and-run) (1) or rapidly expand after a metastable flickering stage (2).

Extended hemifusion diaphragms (HD), in which the two vesicular compartments remain separated by a single lipid bilayer, have been observed in fusion experiments (3). In such a scenario, the initial (fusion) pore is formed near the rim of the extended HD, a rim-pore (3–8). Formation and subsequent expansion of a rim-pore has been observed in a 2010 experiment (see the Supporting Material in Nickolaus et al. (3)). The free energy barrier of rim-pore nucleation has been estimated in molecular simulation studies (5–8). In contrast to the toroidal fusion pore (TFP) (9–12), however, little is known about the free energy landscape of subsequent rim-pore expansion, i.e., dilation of excess HD material, before TFP formation.

Recently, we applied coarse-grained molecular-dynamics (MD) simulations to simulate the SNARE-mediated fusion process between a tensionless bilayer and vesicle (13). In these simulations the formation of a rim-pore was observed (Fig. 1). This nucleated rim-pore remained stable over 1 μs before it eventually expanded into a TFP. Importantly, the observation of such a flickering stage shows that there must be a subsequent expansion barrier. This barrier further suggests that the lateral tension in the HD, which results from the curvature stress in the vesicle, does not suffice to (fully) expand the rim-pore. We emphasize that fusion between a vesicle and a (finite-sized) flat membrane builds up asymmetry in the fused membrane(s) (i.e., differences in leaflet area). This building up or presence of membrane asymmetry is common in in vitro and possibly even in vivo fusion reactions. Such an asymmetry alters the membrane's spontaneous curvature and opposes expansion of both the HD and TFP (Fig. 1). As a result, the stresses subjected to the HD may not suffice to subsequently expand the rim-pore. Thus, aside from the nucleation of the rim-pore, its subsequent expansion also forms an essential free energy barrier in membrane fusion.

Motivated by the observation of a metastable rim-pore in our simulations, we will derive a simple analytical free energy model to explore the free energy landscape of subsequent rim-pore expansion. Here, we will study the shape and corresponding free-energy of the rim-pore; we will investigate how its expansion barrier depends on the size of the HD; and we will calculate the tension required to expand the rim-pore. Finally, we will compare our results with the observations in fusion experiments.

Submitted March 31, 2014, and accepted for publication August 6, 2014.

*Correspondence: hrissel@gwdg.de

Editor: Tobias Baumgart.

0006-3495/14/11/2287/9 $2.00

http://dx.doi.org/10.1016/j.bpj.2014.08.022

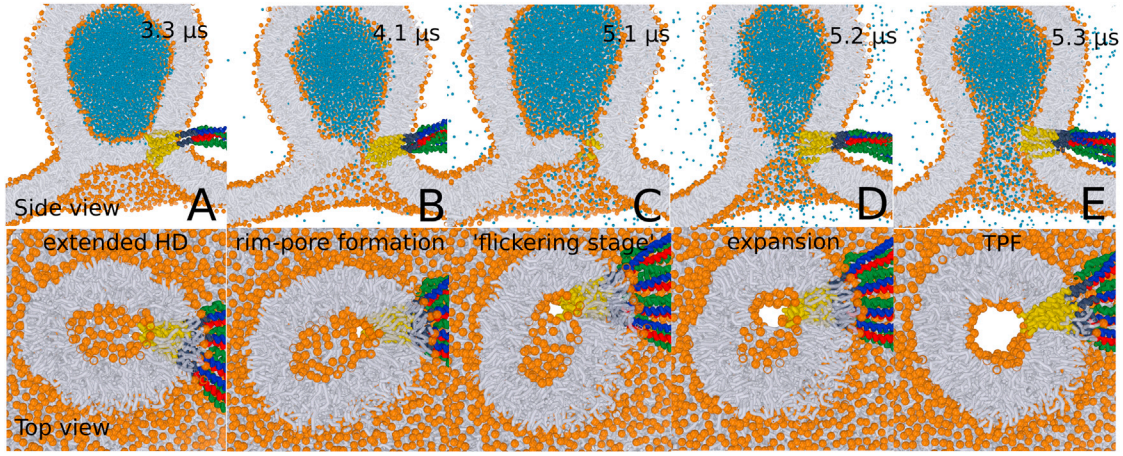

FIGURE 1 Example of the SNARE-mediated fusion process between a 20-nm-sized lipid vesicle and a flat lipid membrane patch (30 × 30 nm). A rim-pore is formed in the 8-nm-sized extended hemifusion diaphragm (HD). Expansion of the rim-pore is associated with a metastable flickering stage. Figure adapted from Risselada and Grubmüller (13). To see this figure in color, go online.

MATERIALS AND METHODS

Free energy model of the rim-pore

Fig. 2 shows our model of the rim-pore.

The shape and free energy of a rim-pore with area A can be obtained by minimizing the free energy integral of

$$F(h,h') = \int_{-a}^{a}\left[\lambda_e\sqrt{1+(dh/dx)^2} + (\lambda_{fp}-\lambda_{hd})\sqrt{1+(df/dx)^2}\right]dx. \quad (1)$$

Under the constraint

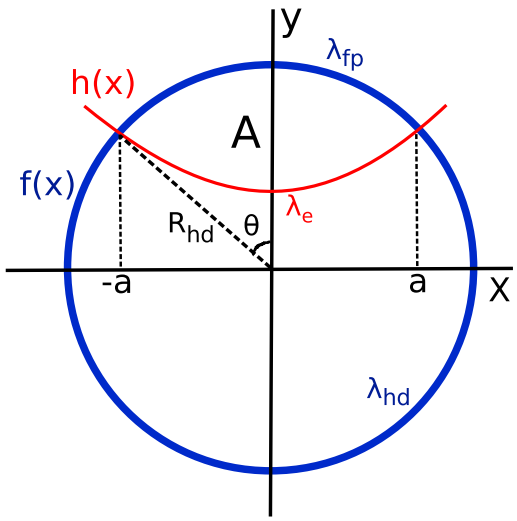

FIGURE 2 Model of the rim-pore, where A is the area of the rim-pore. (*Thick blue line*) Circumference of the HD, $f(x)$. (*Red line*) $h(x)$ is the e-line, i.e., the free membrane edge, with line tension λ_e. The free membrane edge is connected to the circumference of the HD at $h(a) = f(a)$ and $h(-a) = f(-a)$. To see this figure in color, go online.

$$A = \int_{-a}^{a}[h(x)-f(x)]dx = \text{const},$$

where $h(x)$ is the shape equation of the free membrane edge and $f(x)$ the (known) shape of the HD-rim,

$$f(x) = \sqrt{R_{hd}^2 - x^2}.$$

The boundary conditions $x = a$ and $x = -a$ are the two contact points of the membrane edge with the rim of the TFP (the circle). The physics is analogous to the process of wetting in two dimensions, where a droplet is at rest on an interacting plane (Fig. 2). Because F depends on $h(x)$ and $h'(x)$, and not explicitly on x itself, the Euler-Lagrange equation reduces to the so-called Beltrami identity (http://mathworld.wolfram.com/BeltramiIdentity.html). After simplification and substitution of Eq. 2 in the Beltrami identity, one obtains the differential equation

$$dh/dx = \sqrt{\frac{\lambda_e^2 - \left(\lambda h(x) - \left((\lambda_{fp}-\lambda_{hd})C_1 + \lambda C_2 - C_3\right)\right)^2}{\left(\lambda h(x) - (\lambda_{fp}-\lambda_{hd})C_1 + \lambda C_2 - C_3\right)^2}}, \quad (2)$$

where λ is a Lagrange multiplier required to satisfy the area constraint. The constants are

$$C_1 = (\lambda_{fp}-\lambda_{hd})(R/a)\arcsin(a/R),$$

$$C_2 = \left(a\sqrt{R^2-a^2} + R^2\arcsin(a/R) - A\right)/2a,$$

and C_3 is the constant introduced by the Beltrami identity. The solution of Eq. 2, i.e., the shape of the free membrane edge, is the circle

$$x^2 + (y-y_0)^2 = (\lambda_e/\lambda)^2, \quad (3)$$

where y_0 is

$$\sqrt{R^2-a^2} \pm \sqrt{(\lambda_e/\lambda)^2 - a^2}.$$

Making use of the Young equation (14),

$$\lambda_e \cos(\theta) = \lambda_{hd} - \lambda_{fp},$$

where θ is the (relative) contact angle between the e-line and the hd/fp-line, there exists only one circle $h(x)$, which intersects with the circle $f(x)$ at the coordinates $x = a$, $x = -a$ for a given contact angle. The Young relation yields the derivative of the circle $h(x)$ in the coordinate $\pm a, f(a)$, which allows direct calculation of its radius and offset. The free energy of the corresponding rim-pore is subsequently obtained by substitution in Eq. 2.

The area and free energy function of the rim-pore in the vicinity of the expansion barrier, where $h(x)$ can be approximated by a straight line between the points $-a,h$ and a,h, can be modeled as a parametric function of θ (where θ is $0 \rightarrow \pi$):

$$A(\theta) = R_{hd}^2(\theta - \sin\theta\cos\theta), \quad (4)$$

$$F(\theta) = 2R_{hd}\left(\lambda_{fp} - \lambda_{hd}\right)\theta + 2R_{hd}\lambda_e \sin\theta - \sigma A. \quad (5)$$

In this work, we have used $\lambda_e = +5\ k_BT$/nm and $\lambda_{fp} - \lambda_{hd} \pm 1\ k_BT$/nm. The reported values in picoNewtons are rounded. We have neglected a possible (small) contribution coming from the two contact points, i.e., the point where the membrane edge is connected with the TFP. Its relative contribution to the free energy is expected to become rather insignificant when the HD becomes large. We further stress that these models are unable to describe the actual nucleation process of the rim-pore ($A \approx 0$).

F^* and A^* follow from the maximum in Eq. 5: $dF/d\theta = 0$. Equation 5 has a maximum at

$$\theta^* = \arccos\left(\frac{-\lambda_{fp} + \lambda_{hd}}{\lambda_e}\right).$$

Because we study the rim-pore under tensionless conditions ($\sigma = 0$), substitution of θ^* in Eq. 4 and Eq. 5 yields

$$F^*(R_{hd}) = 2R_{hd}\left\{\lambda_e\sqrt{1 - \frac{\left(\lambda_{fp} - \lambda_{hd}\right)^2}{\lambda_e^2}} + \left(\lambda_{fp} - \lambda_{hd}\right)\arccos\left(\frac{-\lambda_{fp} + \lambda_{hd}}{\lambda_e}\right)\right\}, \quad (6)$$

$$A^*(R_{hd}) = R_{hd}^2\left\{\frac{\lambda_{fp} - \lambda_{hd}}{\lambda_e}\sqrt{1 - \frac{\left(\lambda_{fp} - \lambda_{hd}\right)^2}{\lambda_e^2}} + \arccos\left(\frac{-\lambda_{fp} + \lambda_{hd}}{\lambda_e}\right)\right\}. \quad (7)$$

Finally, a first approximation for the effective tension required for rim-pore expansion is obtained by differentiating Eq. 4 and Eq. 5 with respect to θ. This approximation is most accurate in the vicinity of the expansion barrier:

$$\sigma_{\text{eff}}(\theta) = \frac{dF}{dA} = \frac{dF/d\theta}{dA/d\theta} = \frac{\lambda_{fp} - \lambda_{hd} + \lambda_e\cos\theta}{R_{hd}\sin^2\theta}. \quad (8)$$

The exact solution (i.e., taken into account the variable shape of the e-line) can be obtained numerically by calculating the derivative of the $F(A)$ plot obtained by solving the integral in Eq. 2. The presence of tension is not expected to affect the shape of the rim-pore, because the surface free energy of the pore, σA, only depends on its area and not on its shape. The latter is, for example, quite in contrast to a tensed rope that bends because of gravity (a catenary). Finally, we note that $\lambda_{fp} - \lambda_{hd} = 0 \rightarrow A^* = 1/2\ A_{hd}$. Therefore, one can experimentally observe whether $\lambda_{fp} - \lambda_{hd}$ is positive or negative. For example, in Fig. S1 in Nickolaus et al. (3), the HD is clearly under tension whereas the rim-pore is larger than 1/2 A_{hd}. We therefore chose $\lambda_{fp} - \lambda_{hd} = +1\ k_BT$/nm or ~4 pN to estimate the required effective tension (Fig. 5).

Ising model

We performed grid Monte Carlo simulations to obtain the solution of our two-dimensional three-spin Ising model at constant pore area (spin magnetization). The total grid was $80 \times 80 = 6400$ elements, where the circle contained 4872 grid elements. The energy of an Ising spin configuration is given by $E = -J\Sigma d_{ij}s_is_j$, with coupling constant J ¿ 0 (the sum runs over the eight nearest neighbors). If the neighbors are direct neighbors, $d_{ij} = 1$. If the neighbors are diagonal neighbors, $d_{ij} = 0.5$. The spin value of a fusion pore area element was $s = -1$, of an HD element $s = +1$, and the spin of the circular boundary is $s = 0$. These interaction parameters represent the scenario where $\lambda_{fp} - \lambda_{hd} = 0$. To conserve the area of the pore a randomly selected HD element was exchanged with a randomly selected pore element according to the Metropolis criterion. We performed the simulations below phase transition temperature, $J/k_BT = 2$. We performed 5,000,000 MC steps for each pore area, where we defined equilibrium by a plateau in the potential energy of the system.

Molecular simulations

The MD simulations results shown in this article are purely illustrative. We performed our fusion simulations in the presence of four SNARE complexes. The 20-nm-sized POPE vesicle consisted of 2217 lipids, the 30 × 30 nm^2 flat target membrane of 3200 lipids, and 186,363 solvent beads were present. The simulations described in this article were performed with the simulation package GROMACS, Ver. 4.0.5 (15). We used the modeling software MARTINI, Ver. 2.1 (16,17) to simulate the lipids and amino acids. The system was coupled to a constant temperature bath (18), $T = 310$ K, with a relaxation time $\mathcal{T}_T$ of 1.0 ps. The time step used in the simulation was 20 fs. Shifted potentials were used to describe both van der Waals and electrostatic pairwise interactions. In both cases, the neighbor-list cutoff was 1.2 nm and these potentials were gradually shifted to zero when the pairwise distance exceeded 0.9 nm. The neighbor-list was updated every 10 simulation steps. The pressure was weakly coupled (18) to 1 bar with a relaxation time $\mathcal{T}_p$ of 0.5 ps. In analogy to the other studies done with the MARTINI model, the timescales quoted in this work were scaled by a factor of 4 to correct for the four-times faster diffusion rates of water and lipids found in the coarse-grained model (16), with respect to reality. These corrected timescales, however, remain an approximate.

The starting structure of the neuronal SNARE complexes present in our simulations was derived from the x-ray-resolved structure (PDB:3IPD) of the fully assembled SNARE complex by pulling the trans membrane regions (TMRs) of a solvated SNARE complex apart from one other. For simplicity, our model of the SNARE complex only included the resolved SNARE motifs and the complete TMRs of syntaxin and synaptobrevin, consisting of rat syntaxin-1A (residues 188–288), SNAP-25 without the linker region (residues 7–82 and 141–200), and synaptobrevin-2 (residue 26–116). The last two amino acids of the TMR of Syntaxin 1A (residues 287 and 288), which were not resolved in the x-ray structure, were included additionally.

RESULTS

Fig. 4 *A* shows a rim-pore in more detail, and also motivates the simple analytical model developed below. The geometry

involves three different types of boundary lines: the hd-line, i.e., the junction between the diaphragm and the vesicular membrane (*green*); the fp-line, i.e., the upper boundary of the rim-pore corresponding to the partially fused bilayers (*blue*); and the e-line, i.e., the lower boundary of the rim-pore provided by the free edge of the diaphragm (*red*). The total free energy of this system can be described by

$$F(L_{fp}, L_e, A) = (\lambda_{fp} - \lambda_{hd})L_{fp} + \lambda_e L_e - \sigma A, \qquad (9)$$

where L values are the lengths and λ values are the line tensions (forces) of, respectively, the fp-line, hd-line, and e-line. A is the area of the rim-pore, and σ is the lateral tension in the HD. In this model, F is a function of L_{fp}, L_e, and A, which implies that the rim-pore can optimize its shape to optimize its free energy. Note that $\lambda_{fp} - \lambda_{hd}$ is in fact the free energy difference between the HD and (similar-sized) TFP normalized by its circumference. Due to the additional cost of creating a three-bilayer junction, $\lambda_{fp} - \lambda_{hd}$ can become (slightly) negative (9). This implies that the rim of the TPF favorably replaces the HD rim. However, creating the free membrane edge is energetically costly, $\lambda_e >> 0$ and $\lambda_{fp} - \lambda_{hd} << \lambda_e$. This implies that the pore will adopt a shape that represents the best trade-off between the perimeter of the costly free diaphragm edge, L_e, and the (relatively) favorable toroidal fusion pore, L_{fp}. This free energy balance is confirmed by the direct experimental observation of a pore that remains at the rim of the HD (see Fig. S1 in Nickolaus et al. (3)).

The shape of the rim-pore that represents the optimal energy minimum can be determined by the Euler-Lagrange equation of the respective variational problem (see Appendix). It is interesting to note that the above model is similar to the one that describes the formation of lipid domains within the contact area of adhering membranes (19), or the wetting of a curved/deformed surface in two dimensions (20). To study the expansion of a nucleated rim-pore at vanishing HD tension ($\sigma = 0$) in more detail, we assume, for simplicity, that the HD has a circular shape. We further assume that the size and shape of its cross section does not change much during expansion of the rim-pore up to the critical pore size, which defines the position of the expansion barrier of interest.

Closer analysis of our simulations (1) suggests that this assumption is indeed well justified; here, the diameter and shape of the HD seems not significantly affected by the formation/expansion of the rim-pore. Relative magnitudes for $\lambda_{fp} - \lambda_{hd}$ and λ_e can be estimated from Katsov et al. (9). With +5 kT/nm or +20 pN being a commonly cited value for the experimentally derived line-tension of λ_e (21), we choose $\lambda_{fp} - \lambda_{hd} = \pm 1$ kT/nm or ± 4 pN. We emphasize that the precise values chosen for these parameters do not affect the main conclusions we will be able to further draw below. Finally, we note that our rim-pore undergoes a quasi-static expansion. In reality, the membrane viscosity, and to a lesser extent the solvent viscosity, will additionally oppose dynamic expansion of the rim-pore.

Fig. 4 *B* graphically illustrates the pathway of rim-pore expansion under the condition $\lambda_{fp} - \lambda_{hd} = +4$ pN (see Appendix for further detail). The here-derived pathway is quite similar to the one observed in experiments (3). Whenever $\lambda_{fp} - \lambda_{hd} < \lambda_e$,

1. The pore is attracted to the HD rim;
2. The pore is not circular overall in shape; and
3. The pore's free energy is lower than that of an isolated circular pore (i.e., the driving force of the observed attraction to the rim).

The contact angle between the e-line and the fp-line is a direct consequence of their line-tensions (i.e., forces); mechanical equilibrium requires that the net force on the three-junction point equals zero. This force balance is satisfied by the Young equation

$$\lambda_e \cos(\pi - \theta) = \lambda_{fp} - \lambda_{hd},$$

where θ is the (relative) contact angle between the e-line and the fp-line. A negative value of $\lambda_{fp} - \lambda_{hd}$ results in $\theta < 90^\circ$ and a positive value in $\theta > 90^\circ$. Because the three line-tensions are a constant/conserved material property, expansion of the pore conserves the contact angle of the e-line with the circular fp-line (14). Therefore, the shape of the e-line becomes shallower during expansion and is eventually described by a straight line (the expansion barrier). Further expansion of the rim-pore in fact inverts its shape. The relative location of this shape transition depends on the magnitude of $\lambda_{fp} - \lambda_{hd}$ (Fig. 4 *B*). The expansion of the rim-pore can be alternatively visualized by Monte Carlo simulations (Fig. 3).

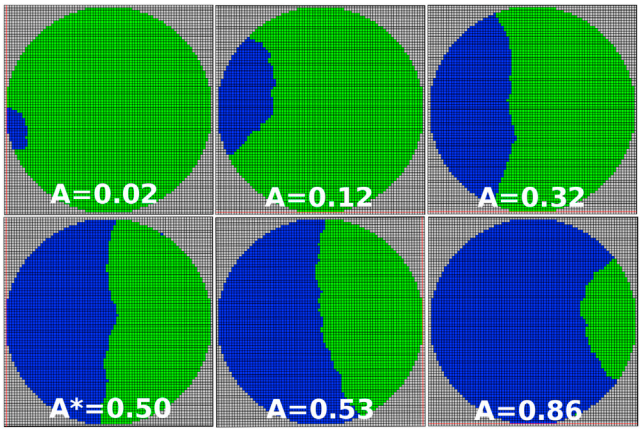

FIGURE 3 Grid Monte Carlo simulation of rim-pore expansion as a function of the relative pore area under the condition $\lambda_{fp} - \lambda_{hd} = 0$. (*Blue*) Rim-pore area; (*green*) remaining HD; and (*gray*) boundary membrane. Note that the free membrane edge adopts concave, linear, and convex shapes during expansion. To see this figure in color, go online.

Fig. 4 *C* compares the free energy of the expanding rim-pore ($R_{hd} = 4$ nm, $\lambda_e = +20$ pN) with a regular, circular pore. The expansion of a (centrally located) circular pore is energetically up-hill up to the point where the HD has completely dilated ($R_{\text{pore}} = R_{hd}$). In contrast, the free energy profile of the rim-pore is only energetically up-hill up to a critical pore size, A^* (Fig. 4 *C*). Once the corresponding barrier F^* is surpassed, subsequent dilation of the HD via expansion of the rim-pore is spontaneous. We emphasize that the shape of the free diaphragm edge L_e is very well approximated by a straight line in the vicinity of the expansion barrier. The expansion barrier stems from the fact that the growth of the free diaphragm edge (e-line) decreases and eventually reverses when the rim-pore expands. In the regime where the expansion of the rim-pore occurs spontaneously, i.e., after the expansion barrier, the now compressive force on the HD and concave shape of the e-line is expected to result in either up- or downward buckling of the remaining HD (see Fig. S1 in Nickolaus et al. (3)).

In contrast to the free energy profile of the TFP (9), the profile of the rim-pore does not display a shallow local free energy minimum that could result in pore-flickering (Fig. 4 *C*). However, so far our model did not include the effect of lateral tension on pore growth.

In a stressed membrane at constant membrane area, a formed pore can initially grow spontaneously despite an unfavorable increase in line-energy because its growth simultaneously reduces the surface free energy of the stressed membrane. Metastability is reached when these two opposing free-energy contributions balance each other (22). Similarly, the metastable rim-pore observed in our simulations (Fig. 1) is most likely explained by the presence of an initial tension in the HD that competes with the line energy of the rim-pore. However, in contrast to a circular pore, the rim-pore may reach its equilibrium size near an expansion barrier. Therefore, in correspondence with our simulations (Fig. 1), such a rim-pore can display a metastable flickering stage before sudden expansion.

We further note that the free energy profile of the rim-pore displays a large relatively flat regime near F^*, especially when the HD becomes larger (Fig. 5). Therefore, substantial size fluctuations (i.e., conductance fluctuations) may occur as a result of thermal fluctuations (flickering). On the other hand, the flickering rim-pore will close if the tension on the HD dissipates during the fusion reaction, for example, due to an increase in leaflet asymmetry in the bulk membrane. The latter would, for example, occur in the presence of multiple (hemi)fusion events. Thus, the experimental observation of flickering fusion pores and subsequent opening/closing (1,2,9) may very well relate to rim-pores as well as TFPs (9–11).

A question that naturally arises is whether fusion proteins, such as SNARE molecules, may actively contribute to rim-pore expansion. Indeed, bystander fusion proteins may exert a squeezing force on the remaining HD rim via the C-termini of their *trans* membrane domains. Such a force causes thinning of the HD rim (hydrophobic mismatch), and thereby increases the line tension λ_{hd} such that $\lambda_{fp} - \lambda_{hd}$ decreases. The latter decreases both the barrier F^* and the critical pore size A^* (Fig.4 *C*). Thus, bystander fusion

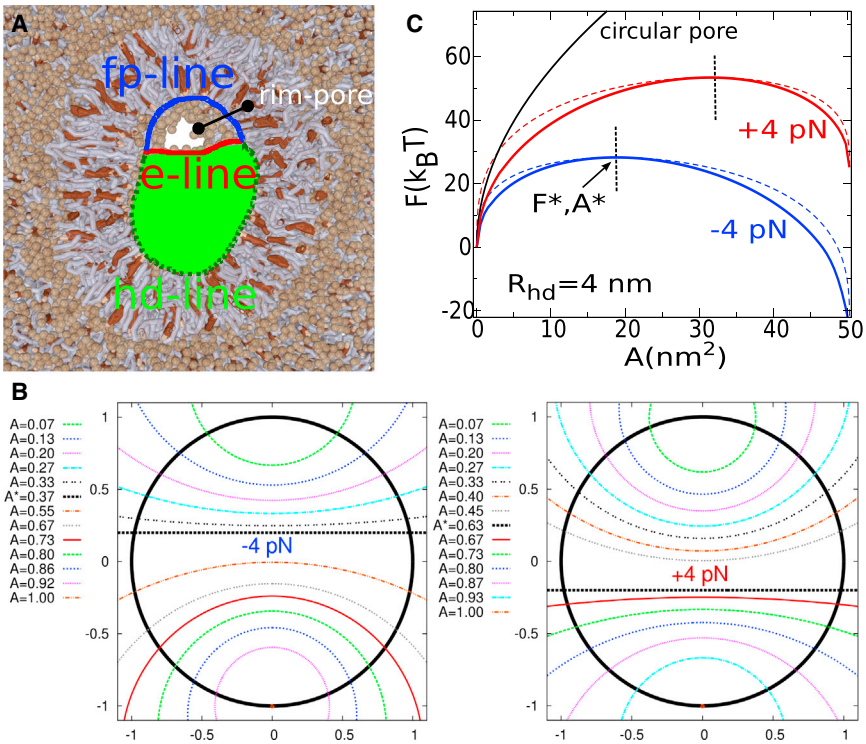

FIGURE 4 (*A*) A rim-pore in detail (13). The geometry involves three different types of boundary lines: the hd-line, i.e., the junction between the diaphragm and the vesicular membrane (*green*); the fp-line, i.e., the upper boundary of the rim-pore corresponding to the partially fused bilayers (*blue*); and the e-line, i.e., the lower boundary of the rim-pore provided by the free edge of diaphragm (*red*). (*B*) Pathway of rim-pore expansion as a function of relative pore area under the conditions $\lambda_{fp} - \lambda_{hd} \pm 1$ kT/nm or ± 4 pN (for further detail, see Appendix). (*Thick, black central circle*) Circumference of the HD (i.e., the hd-line and the fp-line). The shape of the e-line is represented by the intersecting, colored circles. The rim-pore expansion proceeds from top to bottom. (*C*) Free energy of the expanding rim-pore for different values of $\lambda_{fp} - \lambda_{hd}$. (*Black line*) Regular circular pore. (*Dashed lines*) Free energy of a rim-pore; (*straight line*) e-line. To see this figure in color, go online.

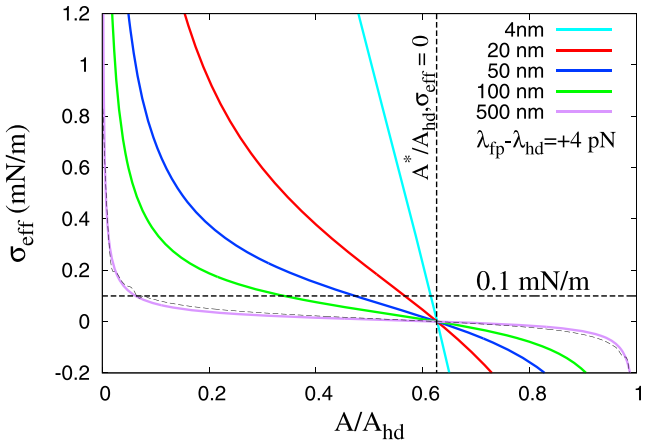

FIGURE 5 Approximation of the effective, external tension, $(\delta F/\delta A)$, required to expand the rim-pore for different values of R_{hd} (see Appendix and Eq. 9). (*Thin black line overlaying purple line*) Exact numerical solution for $R_{hd} = 500$ nm. To see this figure in color, go online.

proteins may actively enhance expansion of the rim-pore, and thereby affect the conductivity of the fusion pore (1).

Does the expansion barrier depend on the size of the formed HD? To address this question, we calculated the barrier of rim-pore expansion, F^*, as a function of HD size, R_{hd} (see Eq. 6). We found that F^* is linearly proportional to R_{hd}. The critical pore size, A^*, increases quadratically with R_{hd}. The implications of such a scaling are substantial. For example, even if $\lambda_{fp} - \lambda_{hd} = -8$ pN, i.e., the HD is thermodynamically rather unstable with respect to the toroidal fusion pore, then $F^* = 3.76\ R_{hd}$ and $A^* = 1.57\ R_{hd}^2$. Therefore, a rim-pore formed in a micrometer-sized HD ($R_{hd} =$ 500 nm) still faces a huge expansion barrier of almost 2000 k_BT. Dilation of such an HD via expansion of an isolated circular pore, however, is substantially more expensive. The latter would require a huge free energy of $2\pi R_{hd} \times \lambda_e$, which is >15,000 k_BT. This explains why an extended HD formed between two giant unilamellar vesicles is unusually stable, because the available bending energy, which is $8\pi\kappa$ ($\approx$500 k_BT) and is independent on vesicle size, does not suffice to dilate the HD.

Intriguingly, even at micrometer length-scales, (spontaneous) rim-pore expansion has been experimentally observed in the presence of an externally induced tension (3). Here, an interleaflet tension was induced in the net negatively charged outer leaflets of giant unilamellar vesicles by introducing divalent charged counterions (electrostatic condensation) (23). This interleaflet tension induces a substantial lateral tension in the microscopic HD, which is estimated to be 10 mN/m (24). It is important to stress that the free energy pumped into such a system is proportional to the tension as well as the total microscopic leaflet area and therefore, even at small tensions, the supplied free energy can become huge, and much larger than the bending energy.

We estimated the tension on the HD required to expand a rim-pore as a function of HD size. We note that the sign of $\lambda_{fp} - \lambda_{hd}$ can be obtained by experimental observation of an expanding rim-pore. If $\lambda_{fp} - \lambda_{hd} = 0$, the barrier is at $A^* = A_{hd}/2$. Thus, if the rim-pore seems larger than $A_{hd}/2$ while the HD remains under tension, such as observed in the experiment (3), then $\lambda_{fp} - \lambda_{hd} > 0$. Based on the obtained microscopy images (3), Eq. 8, and Fig. 4 *C*, we take $\lambda_{fp} - \lambda_{hd} = +4$ pN as an approximation for the line tension in the experiments.

Fig. 5 shows an estimation of the effective tension required for rim-pore expansion, $\sigma_{\text{eff}} = dF/dA$, against the normalized pore area, A/A_{hd} (see Eq. 9). Independent of HD size, this tension is maximal at $A = 0$, i.e., the nucleation of the rim-pore, and gradually decreases up to A^* where it crosses zero. We emphasize, however, that the barrier of pore nucleation is not trivially derived from its line energy (25), and our model is inaccurate at $A/A_{hd} \approx 0$.

Increasing the size of the HD relatively decreases the tension required for subsequent rim-pore expansion (Fig. 5). In fact, tensions of ~0.01 mN/m suffice ($\lambda_{fp} - \lambda_{hd} = +4$ pN) to expand a micrometer-sized HD during the largest part of its expansion. For comparison, an externally applied tension of 0.1 mN/m is commonly reported as a large biological membrane tension. Thus, despite the fact that the microscopic rim-pore faces a huge free energy barrier against expansion, expansion seems promoted by achievable tensions, and is thus experimentally observed (3). Moreover, because the effective tension is maximal near the regime of rim-pore nucleation, an externally applied tension that suffices to nucleate a rim-pore on relatively short timescales will most certainly suffice to subsequently expand the rim-pore, and a metastable rim-pore will not be observed (3,5–7,26). In contrast, rim-pore nucleation in SNARE-mediated fusion can occur on shorter timescales despite a low HD tension because nucleation is additionally facilitated by the local forces that the SNARE molecules impose on the HD via their *trans* membrane domains. Therefore, a metastable rim-pore is more likely observed in SNARE-mediated fusion where nucleation of the rim-pore more easily occurs within the low tension regime (Fig. 1).

DISCUSSION

Kiss-and-run: rim-pore versus toroidal fusion pore

In contrast to the process of rim-pore closing, which has been observed in MD simulations (8), the process of TFP closing directly relates to the process of membrane fission where the inside of a fission neck (the TFP) is dehydrated to form a stalk intermediate. Membrane fission, however, is GTP-driven and requires the presence of Dynamin, which forms a spiral around the neck of the TFP. The latter indicates that complete closing of the TFP very likely faces a substantial free energy barrier. The so-called kiss-and-run events observed in synaptic fusion (1), where the fusion

pore completely closes after opening, are difficult to envisage for a TFP in the absence of the fission machinery. Instead, in these systems the membrane tension may be sufficiently low such that the nucleated HD can expand to a metastable size before rupturing (5). A recent in vitro fusion experiment illustrated that the survival of the HD severely limits the rate of the synaptic fusion reaction (27). These experiments further illustrated that the interplay among SNARE molecules, Complexin, and Synaptotagmin-1 prevents formation/stabilization of the HD (27). Corruption of this pathway may lead to stabilization/expansion of the nucleated HD and result in the here-described rim-pore phenomena. Further, the presence of molecules that oppose membrane rupture, such as, e.g., cholesterol, enhance survival of the nucleated hemifusion diaphragm and thereby facilitate expansion of the HD toward a more metastable size. Because the subsequent rupture of such an HD involves rim-pore formation, the presence of cholesterol is thus expected to enhance the propensity of pore-flickering (28). Finally, fluctuations in tension will discern between closure or complete opening of the rim-pore.

Formation and dilation of the microscopic hemifusion diaphragm: implications for biological membrane fusion

The estimated free energies at microscopic length scales raises the question whether cellular organisms, in their attempt to minimize energetic costs, would favor a fusion mechanism that proceeds via formation of a micrometer-sized HD and requires subsequent HD dilation. At these length scales the bending energy stored in the membrane(s) would not suffice to dilate the HD, and expansion of the rim-pore requires up to several thousands of k_BT. It is also important to note that the excess area of the HD observed in, for example, vacuole fusion is substantial with respect to the area of the bulk membrane, and therefore the uptake of HD material by the bulk membrane(s) would require a substantial additional free energy. Moreover, the formation/nucleation of an HD itself, as well as its subsequent expansion toward a microscopic size, is also opposed by a similar, substantial free energy barrier (9,23). It is very unlikely that biological membrane fusion would spend a huge amount of energy to form a microscopic HD only to spend another huge amount of energy for its subsequent dilation. Thus, it is intuitive that biological membrane fusion circumvents both the formation and subsequent dilation of the (microscopic) HD.

The microscopic HD formed in homotypic vacuole fusion has been observed to cleave off as a large deflated vesicle that remains within the fused structure (29,30)—quite in contrast to the process of rim-pore expansion observed in recent experiments (3). The occurrence of an alternative pathway in in vivo fusion is not coincidental nor surprising, given the illustrated energy crisis of HD formation/dilation on these cellular length scales.

There are three possible scenarios to explain the observed dilation of an HD in homotypic vacuole fusion:

1. Curvature generating proteins, such as BAR-domains, drive the expansion of the rim-pore, i.e., dilation of the HD. In such a scenario, the deflated vesicle is a bud formed in the HD (the process of membrane budding and tubulation). However, such a scenario would be extremely costly, because aside from expanding the rim-pore, a large additional energetic cost would be incurred in creating additional membrane curvature in the HD.
2. The HD cleaves off as an isolated membrane disk via formation/propagation of a crack formed along the rim of the HD. In such a scenario, the deflated vesicle results from the obtained isolated disk that folds up into a vesicle (31–33). In principle, spontaneous crack propagation can occur when $\lambda_{fp} - \lambda_{hd} + \lambda_e > 0$. However, whenever $\lambda_e > 0$, the system tends to minimize the length of the free membrane edge and a rim-pore is formed. In contrast, if $\lambda_e \leq 0$, the disk will never fold up into the observed vesicle (31,33). Moreover, the disk-to-vesicle transition is expected to yield a spherical vesicle that is under osmotic stress (34), rather than a deflated vesicle.
3. The formed internal vesicle does not result from an HD, but from an alternative fusion intermediate (30).

We explore Scenario 3, because Scenario 1 faces a large energy crisis, whereas Scenario 2 most likely results into a reaction pathway that seems not to conform with the experimental observation of an instantaneously formed deflated vesicle (29,30). The experimental observations of vacuole fusion further suggest that the formed HD is comprised of two membranes, i.e., an extended inverted micelle intermediate (IMI) (Fig.6 *A*), rather than a single membrane (29,30). MD simulations and self-consistent field theory in fact support the formation of such an intermediate (13,35,36). The

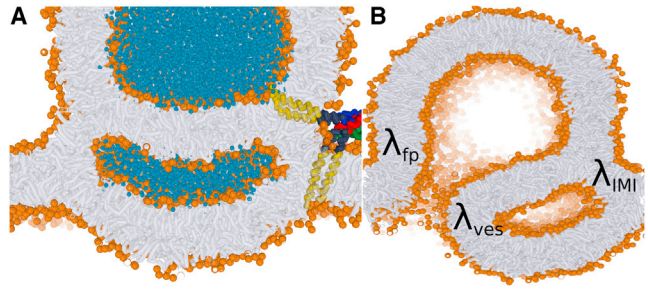

FIGURE 6 Alternative pathways for the dilation of hemifusion intermediates. (*A*) A double HD or inverted micelle intermediate (IMI) formed during fusion between a pure POPE membrane and vesicle. Note the conserved amount of isolated lipid material that is entrapped within the inner leaflet of the inverted micelle. Therefore, quite in contrast to the HD, the bulk membrane is essentially unable to absorb excess IMI material. (*B*) Initial crack present near the edge of the IMI, i.e., the four-bilayer junction. Propagation of the crack will cleave off a deflated vesicle. To see this figure in color, go online.

formation of the deflated vesicle can be understood as a crack that linearly propagates along the rim of the double HD and which cleaves it off as a deflated vesicle (Wang et al. (29), Wickner (30); and see Fig. 6 *B*). This explains why the cleaved-off, deflated vesicle seems instantaneously formed in the experiment (29). In such a scenario, formation of the costly free membrane edge is not required because the two membranes can associate into the relatively favorable bent membrane, i.e., the rim of the deflated vesicle. During propagation, the free energy of the crack changes simultaneously with

$$L_{\mathrm{crack}}\left(\lambda_{fp} - \lambda_{\mathrm{IMI}} + \lambda_{\mathrm{ves}}\right),$$

where L_{crack} is the length of the crack, and λ_{fp}, λ_{IMI}, and λ_{ves} are the line tensions of the toroidal fusion pore, double-membrane junction, and vesicle rim, respectively. Spontaneous crack propagation requires s$\lambda_{fp} - \lambda_{\mathrm{IMI}} + \lambda_{\mathrm{ves}} < 0$. In contrast to the HD, when $\lambda_{\mathrm{ves}} \leq 0$, the equivalent of a rim-pore is not formed, because the bulk membrane is unable to absorb the entrapped, excess material of the IMI (Fig. 6). Thus, crack propagation is the only scenario to dilate an IMI without rupturing the individual membranes. However, we emphasize that λ_{IMI} should be (initially) negative to from a thermodynamically stable IMI, via a so-called stalk elongation mechanism (13,35). We note that $\lambda_{\mathrm{IMI}} < 0$ corresponds to the induction of a (local) inverted hexagonal phase regime. The latter may very well explain why the concentration of inverted hexagonal-phase former membrane components increases along the perimeter of the contact interface before membrane fusion, forming a so-called vertex ring (30). It is thus plausible that the vertex ring is formed to both drive and guide the formation and subsequent elongation of the stalk.

An important indication of stalk elongation is the occurrence of (transient) leakage during progression of fusion (35,36). MD simulations suggest that rupture of one of the encircled membrane fractions may occur before formation of the IMI is completed, i.e., before the stalk has fully encircled the vertex ring (37). Such a premature rupture results in leaky fusion (37). In correspondence with the IMI pathway, the reaction pathway of vacuole fusion is rather susceptible to leakage. For example, perturbing the fusion pathway by overexpressing a single SNARE protein results in leaky fusion (38). In summary, formation of a double HD and subsequent IMI dilation via vesicle formation provides a very plausible scenario to explain these experimental observations.

Further, because the (initial) condition $\lambda_{\mathrm{IMI}} < 0$ is essential for IMI formation, the driving force of crack formation (vesicle budding) likely stems from the combined favorable creation of a TFP (λ_{fp}) and the inflation of the cleaved-off vesicle edge (λ_{ves}). Here, the molecular forces exerted by nearby fusion proteins are likely crucial in satisfying this free energy balance. In contrast to the rim-pore, the crack propagation mechanism does not face an HD size-dependent free energy barrier, nor is it opposed by an additional energetic cost for uptaking excess HD area. The latter may become a substantial advantage when fusion is associated with cellular length scales and a relatively large excess membrane area such as in vacuole fusion.

The here-illustrated scenario can be experimentally validated by the addition of distinct fluorescence lipid dyes on both the inner and outer leaflet of the fusing vacuoles. The lipid dyes that are added to the outer leaflet of the vacuole should end up within the inner leaflet of the formed internal vesicle and vice versa.

We acknowledge grant No. SFB803/B2 for financial support.

REFERENCES

1. Alabi, A. A., and R. W. Tsien. 2013. Perspectives on kiss-and-run: role in exocytosis, endocytosis, and neurotransmission. *Annu. Rev. Physiol.* 75:393–422.

2. Chanturiya, A., L. V. Chernomordik, and J. Zimmerberg. 1997. Flickering fusion pores comparable with initial exocytotic pores occur in protein-free phospholipid bilayers. *Proc. Natl. Acad. Sci. USA.* 94:14423–14428.

3. Nikolaus, J., M. Stöckl, …, A. Herrmann. 2010. Direct visualization of large and protein-free hemifusion diaphragms. *Biophys. J.* 98:1192–1199.

4. Kozlovsky, Y., L. V. Chernomordik, and M. M. Kozlov. 2002. Lipid intermediates in membrane fusion: formation, structure, and decay of hemifusion diaphragm. *Biophys. J.* 83:2634–2651.

5. Gao, L., R. Lipowksy, and J. Shillcock. 2008. Tension-induced vesicle fusion: pathways and pore dynamics. *Soft Matter.* 4:1208–1214.

6. Grafmüller, A., J. Shillcock, and R. Lipowsky. 2007. Pathway of membrane fusion with two tension-dependent energy barriers. *Phys. Rev. Lett.* 98:218101.

7. Grafmüller, A., J. Shillcock, and R. Lipowsky. 2009. The fusion of membranes and vesicles: pathway and energy barriers from dissipative particle dynamics. *Biophys. J.* 96:2658–2675.

8. Nishizawa, M., and K. Nishizawa. 2013. Molecular dynamics simulation analysis of membrane defects and pore propensity of hemifusion diaphragms. *Biophys. J.* 104:1038–1048.

9. Katsov, K., M. Müller, and M. Schick. 2004. Field theoretic study of bilayer membrane fusion. I. Hemifusion mechanism. *Biophys. J.* 87:3277–3290.

10. Jackson, M. B. 2009. Minimum membrane bending energies of fusion pores. *J. Membr. Biol.* 231:101–115.

11. Ryham, R. J., M. A. Ward, and F. S. Cohen. 2013. Teardrop shapes minimize bending energy of fusion pores connecting planar bilayers. *Phys. Rev. E Stat. Nonlin. Soft Matter Phys.* 88:062701.

12. Haluska, C. K., K. A. Riske, …, R. Dimova. 2006. Time scales of membrane fusion revealed by direct imaging of vesicle fusion with high temporal resolution. *Proc. Natl. Acad. Sci. USA.* 103:15841–15846.

13. Risselada, H. J., and H. Grubmüller. 2012. How SNARE molecules mediate membrane fusion: recent insights from molecular simulations. *Curr. Opin. Struct. Biol.* 22:187–196.

14. Bormashenko, E. 2009. Wetting of flat and rough curved surfaces. *J. Phys. Chem. C.* 113:17275–17277.

15. Hess, B., C. Kutzner, …, E. Lindahl. 2008. GROMACS 4: algorithms for highly efficient, load-balanced, and scalable molecular simulation. *J. Chem. Theory Comput.* 4:435.

16. Marrink, S. J., H. J. Risselada, …, A. H. de Vries. 2007. The MARTINI force field: coarse-grained model for biomolecular simulations. *J. Phys. Chem. B.* 111:7812–7824.

17. Monticelli, L., S. K. Kandasamy, …, S. J. Marrink. 2008. The MARTINI coarse-grained force field: extension to proteins. *J. Chem. Theory Comput.* 4:819–834.

18. Berendsen, H. J. C., J. P. M. Postma, …, J. R. Haak. 1984. Molecular-dynamics with coupling to an external bath. *J. Chem. Phys.* 81:3684–3690.

19. Weikl, T. R., and R. Lipowsky. 2004. Pattern formation during T-cell adhesion. *Biophys. J.* 87:3665–3678.

20. Rascón, C., and A. O. Parry. 2000. Geometry-dominated fluid adsorption on sculpted solid substrates. *Nature.* 407:986–989.

21. Portet, T., and R. Dimova. 2010. A new method for measuring edge tensions and stability of lipid bilayers: effect of membrane composition. *Biophys. J.* 99:3264–3273.

22. Tolpekina, T. V., W. K. den Otter, and W. J. Briels. 2004. Simulations of stable pores in membranes: system size dependence and line tension. *J. Chem. Phys.* 121:8014–8020.

23. Warner, J. M., and B. O'Shaughnessy. 2012. The hemifused state on the pathway to membrane fusion. *Phys. Rev. Lett.* 108:178101.

24. Warner, J. M., and B. O'Shaughnessy. 2012. Evolution of the hemifused intermediate on the pathway to membrane fusion. *Biophys. J.* 103:689–701.

25. Tolpekina, T. V., W. K. den Otter, and W. J. Briels. 2004. Nucleation free energy of pore formation in an amphiphilic bilayer studied by molecular dynamics simulations. *J. Chem. Phys.* 121:12060–12066.

26. Shillcock, J. C., and R. Lipowsky. 2005. Tension-induced fusion of bilayer membranes and vesicles. *Nat. Mater.* 4:225–228.

27. Diao, J., P. Grob, …, A. T. Brunger. 2012. Synaptic proteins promote calcium-triggered fast transition from point contact to full fusion. *eLife.* 1:e00109.

28. Wang, N., C. Kwan, …, F. W. Tse. 2010. Influence of cholesterol on catecholamine release from the fusion pore of large dense core chromaffin granules. *J. Neurosci.* 30:3904–3911.

29. Wang, L., E. S. Seeley, …, A. J. Merz. 2002. Vacuole fusion at a ring of vertex docking sites leaves membrane fragments within the organelle. *Cell.* 108:357–369.

30. Wickner, W. 2010. Membrane fusion: five lipids, four SNAREs, three chaperones, two nucleotides, and a Rab, all dancing in a ring on yeast vacuoles. *Annu. Rev. Cell Dev. Biol.* 26:115–136.

31. Helfrich, W. 1974. The size of bilayer vesicles generated by sonication. *Phys. Lett. A.* 50A:115–116.

32. Markvoort, A. J., K. Pieterse, …, P. A. Hilbers. 2005. The bilayer-vesicle transition is entropy driven. *J. Phys. Chem. B.* 109:22649–22654.

33. Hu, M., D. H. de Jong, …, M. Deserno. 2013. Gaussian curvature elasticity determined from global shape transformations and local stress distributions: a comparative study using the MARTINI model. *Faraday Discuss.* 161:365–382, Discussion 419–459.

34. Markvoort, A. J., P. Spijker, …, P. A. Hilbers. 2009. Vesicle deformation by draining: geometrical and topological shape changes. *J. Phys. Chem. B.* 113:8731–8737.

35. Katsov, K., M. Müller, and M. Schick. 2006. Field theoretic study of bilayer membrane fusion: II. Mechanism of a stalk-hole complex. *Biophys. J.* 90:915–926.

36. Schick, M. 2011. Membrane fusion; the emergence of a new paradigm. *J. Stat. Phys.* 142:1317.

37. Risselada, H. J., C. Kutzner, and H. Grubmüller. 2011. Caught in the act: visualization of SNARE-mediated fusion events in molecular detail. *ChemBioChem.* 12:1049–1055.

38. Südhof, T. C. 2007. Membrane fusion as a team effort. *Proc. Natl. Acad. Sci. USA.* 104:13541–13542.